Technical Note

Landslides
DOI 10.1007/s10346-025-02615-7
Received: 1 April 2025
Accepted: 22 August 2025

Agnese Innocenti · Anne-Sophie Mreyen · Léna Cauchie · David Caterina · Valmy Dorival · Yawar Hussain · Hans-Balder Havenith · Veronica Pazzi

Geophysical reconnaissance of the *Pays de Herve* landslides, Belgium: case study of three active paleo-slides in a dissected tableland

Abstract The *Pays de Herve* region in East Belgium is characterised by widespread slope instability. Some of these Quaternary paleo-landslides are still active, showing subsidence phenomena that can be related to the presence of weak subsurface materials such as clays (locally topped by weathered chalk) overlying a discontinuous sand-silt layer. This study provides a detailed characterisation of three active landslides in the area, with a particular focus on the Manaihan landslide, which is the most active and has also caused damage to surrounding buildings. To investigate these landslides, an integrated geophysical approach was applied, combining electrical resistivity tomography, P-wave seismic refraction, multichannel analysis of surface waves, and microseismic ambient noise measurements (H/V analysis). Each method has intrinsic limitations, but their combined use allowed for a comprehensive analysis of the sliding surfaces. While the first three techniques provided detailed information on limited sectors of each landslide, the ambient noise measurements enabled the coverage of the entire landslide areas. This integrated approach, combining microseismic ambient noise frequency analysis, allowed for a detailed mapping of the Manaihan landslide's subsurface and the creation of a 3D geological model of the site. The results align well with the geophysical imagery collected, allowing the precise identification of the landslide bases and enhancing the understanding of the subsurface structure in the *Pays de Herve* region.

Keywords Electrical resistivity tomography · Seismic refraction tomography · MASW · H/V amplitude

Introduction

Shallow landslides are instability phenomena that affect the uppermost layers of the subsurface. These events are particularly common in the hilly and mountainous areas of the planet (Montrasio and Valentino 2007). They are often triggered by intense or prolonged rainfall. The rising prevalence of extreme weather events, driven by climate change, amplifies both the frequency and intensity of these landslides, leading to even greater damage. Water infiltration plays a critical role by increasing the pressure of the pore water, which reduces the shear strength of the soil, ultimately destabilising the slope (Persichillo et al. 2017).

Most shallow landslides mainly involve surface debris, and their sliding surfaces often develop along layers parallel to the slope with differing hydraulic and mechanical properties. The geology and geomorphology of the slope play a fundamental role in triggering these movements, which are typically translational slides (c.f., Hungr et al., 2014). They are, in fact, set on soils with low cohesion, high permeability, and often at the contact between impermeable and permeable layers. Identifying the trigger mechanisms and the shear surface is crucial to understand the future evolution of these phenomena. However, characterising superficial landslides set in sandy-loamy-clay soils is somewhat complicated, as the slip surface is not always well delineated (Yalcin 2007; Chandler 2020; Vivoda Prodan et al. 2023; Innocenti et al. 2023).

The application of geophysical techniques for characterising unstable slopes is firmly established within the scientific community, having regard to the intrinsic limitations of each method (cf., Pazzi et al., 2019). Among the most commonly used techniques are Electrical Resistivity Tomography (ERT), active and passive seismic surveys, and ground penetration radar (GPR) (Mreyen et al. 2021; Lapenna and Perrone 2022; Calamita et al. 2023; Kabeta et al. 2023; Innocenti et al. 2023). However, each geophysical method is typically sensitive to a single physical property of the terrain, which may vary in time and space (Whiteley et al. 2019). The ERT technique is highly sensitive to the presence of water, as it significantly reduces resistivity, which in turn is also affected by other factors such as salinity, temperature, and chemical composition. Furthermore, both vertical and horizontal resolution decrease with depth (Pazzi et al. 2019). A major limitation of seismic refraction lies in its inability to detect so-called "blind zones", which occur when there is a low-velocity contrast between layers or when velocity inversions are present, i.e., when seismic velocity does not increase progressively with depth (Redpath 1973). Similarly, passive seismic methods struggle to provide accurate imaging of subsurface geometry in the absence of significant seismic impedance contrasts. In rigid environments, such as compact rock or highly homogeneous soils, the impedance contrast may be too low to generate a meaningful peak. In areas with surface irregularities, such as hills, slopes, the local seismic response is also affected by topographic effects, which can amplify ground motion due to terrain geometry. In the presence of multiple interfaces or weak contrasts, the peak may become damped or split into multiple peaks, making interpretation more challenging (SESAME 2004). Therefore, a single geophysical technique alone cannot provide a complete overview, and the integration of several techniques can help overcome many individual limitations. Recent studies have emphasised the benefits of integrated, multi-method approaches. For instance, the joint use of ERT and seismic techniques has been shown to improve the interpretation of subsurface structures by combining sensitivity to both electrical and mechanical properties (Grandjean et al. 2009; Bièvre et al. 2012). Such multi-parameter strategies, whether applied qualitatively or through joint inversion frameworks, help reduce

the non-uniqueness of results and provide a more robust understanding of landslide dynamics (Uhlemann et al. 2017). Electrical and seismic refraction tomographies, as well as the analysis of the dispersion of surface waves, are often only capable to characterise a limited portion of the landslide subsurface (directly below the survey line), due to instrumental constraints (e.g., the finite length of the cables). Single-station seismic noise measurements, even though point measurements, can be performed with a sufficient number of acquisitions as to cover the whole area under investigation (Castellaro 2016; Pazzi et al. 2017; Mreyen et al. 2021; Innocenti et al. 2023). When the single-station seismic noise measurements are elaborated according to the Horizontal to Vertical Spectral Ratio (HVSR or H/V Nakamura 1989), two main hypotheses have to be considered: (a) the superficial layer can be assumed homogeneous, and (b) the shear wave velocity increases with depth due to gravity compaction. In those cases, all H/V curves collected over a site can be elaborated together, converting them from the H/V-frequency into the H/V-depth domain, thus creating a section (i.e., a contour plot of the H/V curves) showing the amplitude variation of H/V with depth (Ibs-von Seht and Wohlenberg 1999; Delgado et al. 2000; Castellaro 2016; Pazzi et al. 2017, 2018; Sgattoni and Castellaro 2020; Song et al. 2021; Seitone et al. 2025). If all the conditions are met, these sections allow to identify the interfaces between layers.

The *Pays de Herve* area in eastern Belgium is severely affected by both active and quiescent paleo-landslides. Their movements have been known since the 1990 s (Demoulin and Glade 2004; Demoulin and Chung 2007; Preuth et al. 2010), while some of them have been reactivated by human activity (infrastructure construction) and/or rainfall (notably the Manaihan landslide). The Herve landslides developed in Cretaceous deposit, mainly composed clays (Vaals Formation) with a thickness between 10 and 30 m (see the "The study area" section for more details), lying on top of sands and silts (Aachen Formation) with a thickness ranging from 0 to 10 m (Demoulin and Glade 2004). As in the *Pays de Herve* area, more than 50 landslides have been identified, it is favourable to use less costly and non-invasive methods that allow a larger area to be studied than the one that can be prospected by geotechnical investigations.

Although it is known that it is difficult to identify the shear surface by using geophysical techniques alone in pure soft sedimentary contexts characterised by a high sand and clay content, this study focuses on the integration four different geophysical methods to characterise three landslides (i.e., the Sérezé Landslide, the Thimister Landslide, and the Manaihan Landslide) in the *Pays de Herve* area. In particular, ERT, Seismic Resistivity Tomography (SRT), Multi-channel Analysis of Surface Waves (MASW), and the Horizontal to Vertical Spectral Ratio (HVSR or H/V) technique were combined to identify horizons and try to differentiate geological contacts from landslide ones. In this context, several HVSR measurements were performed and validated with a few number of ERTs, SRTs, and MASWs. Moreover, the H/V data were used to create two-dimensional sections (Pazzi et al. 2017; Song et al. 2021; Seitone et al. 2025) to achieve greater slope detail. In fact, despite the assumptions listed above, this methodology has shown that it can also be used in the context of slope instability (Panzera et al. 2012): a landslide can be considered a loose material having a certain velocity, and the sliding plane can represent a seismic impedance contrast at the contact between two materials having different velocities. Thanks to a sufficiently large data coverage at the Manaihan landslide, the survey was pursued further, resulting in a 3D subsurface model of the site. This study highlights the practical and scientific relevance of integrating multiple geophysical techniques to investigate landslides in soft sedimentary environments, such as those found in the *Pays de Herve* region, in order to obtain a reliable model that can be used in the future to analyse slope movements and understand the underlying triggering mechanisms. Traditional geotechnical investigations are often limited in spatial coverage and can be invasive and costly. By contrast, the combination of ERT, SRT, MASW, and H/V techniques provides a non-invasive and cost-effective means to obtain both localised detail and broader spatial insight (Lin et al. 2015). The ability to identify lithological contrasts and possible slip surfaces across entire landslides—confirmed by H/V sections and integrated into 3D geological models—offers a significant advancement in landslide characterisation and hazard assessment (Merritt et al. 2014). Moreover, the validation of H/V data through active geophysical methods enhances the reliability of the interpretations, supporting the potential use of this integrative approach in similar geological settings worldwide.

The study area

The *Pays de Herve*, region of Battice in E-Belgium, can be described as a "dissected tableland" with a moderate relief, generally presenting slope angles of less than 15°. The area is located close to the northern part of the Hockai Fault Zone (HFZ), a 42 km long seismogenic fault zone that is situated in the eastern part of Belgium (regions Battice to Malmedy-Waimes) and marked by multiple sections, fault scarps, and landslides (Mreyen et al. 2018). A part of the northern HFZ was formerly called the "Minerie Graben", limited to its East by the "Ostend fault", (Forir 1905; Ancion and Evrard 1957), which supposedly ruptured several times due to seismic activity of the HFZ (Demoulin et al. 2003). More than 50 landslides developed in an Upper Cretaceous soft deposits within the northern part of the HFZ or near to it, with numerous older (including a few quite large, > 1 Mio.m^3) landslide dated to an age of 150 A.D., according to Demoulin et al. (2003). A few recent and even ongoing re-activations of some of the landslides have also been described, e.g., by Demoulin et al. (2003); Demoulin and Glade (2004), and Demoulin and Chung (2007). The Manaihan Landslide (marked with M in Fig. 1), studied and discussed by Demoulin and Glade (2004), is the best monitored paleo-slide of the region in terms of present surface displacements; the first reactivations were supposedly observed during intense rainfall periods in the 13^{th} – 14^{th} century. Still today, the slope is affected by instability and subsidence phenomena, most probably related to anthropogenic loading in combination with prolonged rainfall periods (Demoulin and Glade 2004).

The widespread slope instability in the *Pays de Herve* region can be related to the presence of weak subsurface materials: sand-silt layers of the Aachen Formation underlying the clays and marls of the Vaals Formation. This geological setting is considered unfavourable, especially with the occurrence of possible liquefaction phenomena, i.e., quicksand behaviour (as suggested by Demoulin et al. (2003), and observed by Graulich (1969), for the Aachen sands). Whether the trigger mechanisms of the slope failures were of seismic, climatic, or mixed nature remains unclear; however, the spatial distribution of the deep mass movements suggests a seismic origin (Demoulin et al. 2003). The seismicity of the region can be

Linked to the eastern border fault of the seismically active HFZ and the close location of the epicentre of the historic 1692 Verviers earthquake (cf., Alexandre et al., 2008). In order to explain the likely simultaneous development of all the Battice landslides, Demoulin et al. (2003) suggested repeated intense short-term rain in combination with seismic activity as the most realistic triggering scenario.

The geology of the studied region consists of a folded Paleozoic basement, the Carboniferous Houiller shales, underlying the sub-horizontal Cretaceous cover layers that form the characteristic tableland of the region. The Herve landslides formed in these Cretaceous deposits that can be subdivided into three formations (from old to young): the Aachen sands, the Vaals clays, and the Gulpen chalk. Figure 1 illustrates the geological context in relation to the landslides mapped by Demoulin and Glade (2004). The Aachen formation (Middle Santonian) at the base of the Cretaceous layers formed in a shallow marine milieu and is characterised by fine sands interlayered with coarser sands and clays (Demoulin et al. 2003). The younger Vaals formation (Lower Campanian) is marked by glauconiferous clays and marls (gray-green colored *Smectites de Herve*), but silty sand layers are also present in this formation. According to Demoulin et al. (2003), the Aachen formation is characterised by a maximum thickness of 10 m, while the overlying Vaals formation can reach a thickness of 25 m in our study area. The chalks of the marine Gulpen formation (Upper Campanian) show only a limited presence in our study area, and are found in a rather highly weathered state in the form of clay layers mixed with flints (Demoulin et al. 2003).

The Sérezé and Thimister Landslides (marked with S and T, respectively, in Fig. 1) rank among the biggest slope failures of the Battice region. The sites are located east of the eastern border fault

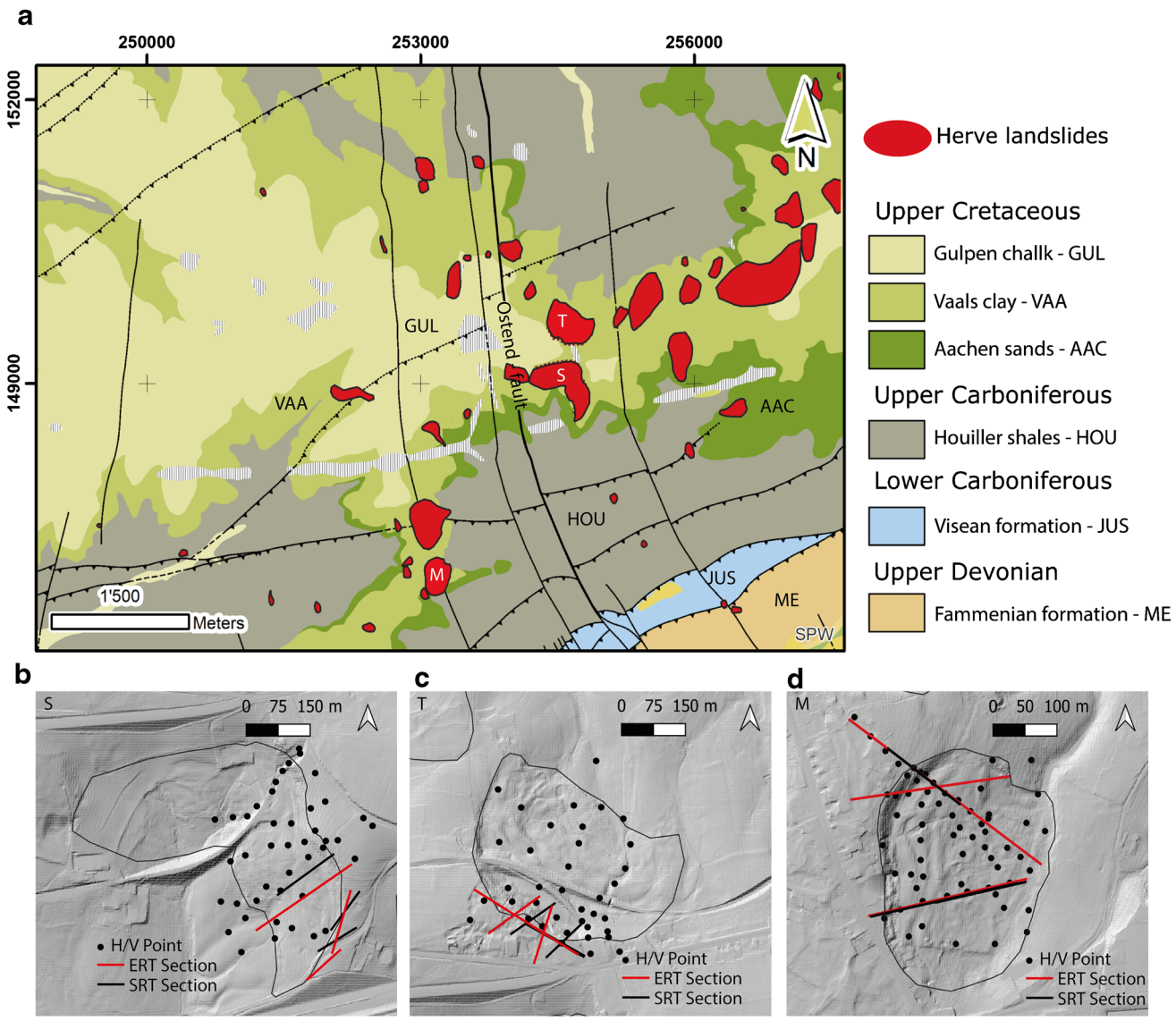

Fig. 1 **a** Geological context of the *Pays de Herve* after Barchy and Marion (2000) and Laloux et al. (1996) with the Ostend fault and paleo-landslides mapped by Demoulin and Glade (2004); T, Thimister landslide; S, Sérezé landslide; and M, Manaihan landslide. **b**, **c**, and **d** hillshade analysis of Sérezé landslide, Thimister landslide, and Manaihan landslide, respectively, with the corresponding geophysical measures

of the HFZ and only 160 m apart. The Sérezé Landslide is situated north along the highway Aachen-Liege. The affected area is dissected into two parts by an ancient railway. The southern part is probably the most active part of the landslide. Landslide Sérezé covers a surface of 16.9 ha and is characterised by very gentle slope angles below 15°, with the exception of the scarp area that reaches a height of ~15 m and the slope steepens to a maximum of 40°. Landslide Thimister can be limited to an area of 13.9 ha and presents an even steeper detachment zone of ~20 m height with slope angles greater than 40°. Both sites are crossed by an old railway track that nowadays is used as a cycling trail. The surface of the landslides is marked by typical hummocky structures that developed in the Vaals clays; in this area, no outcrops of the underlying Aachen formation can be found on the surface.

The Manaihan landslide (marked with M in Fig. 1) is situated south of Battice, on a gently sloping (~ 4°) eastern flank of a south-striking secondary ridge of the Herve tableland. It has a width of about 400 m and a length of 250 m, thus covering an area of about 7 ha. The landslide area is almost completely covered by meadows. Behind the head scarp, a row of houses is present, some of which were affected by recent sliding activity (since 1990). In addition, a factory ("Café Liégeois") was temporarily shut down because of these movements. The Manaihan landslide is located in the upper Cretaceous Vaals clays, which can be up to 12 m thick. These clays rest on 4 m of fine sands from the Cretaceous Aachen Formation (Demoulin and Glade 2004). Probably the liquefaction phenomena that occurred in the area (Demoulin et al. 2003) led to a mixing of the Aachen sands with the Vaals clays. As can be seen from the geological map (Fig. 1), the Aachen sands tend to disappear to the west. Below it lies the Houiller shales formation of the Upper Carboniferous.

Materials and methods

In this study, the subsurface of three of the *Pays de Herve* slope instabilities were studied using an integrated approach of electrical resistivity measurements, active seismic (interpreted in the form of tomographies and multi-channel analysis of surface waves), and passive seismic techniques (single-station H/V). In the following, the applied geophysical methods are briefly recalled.

Electrical resistivity measurements

The Electrical Resistivity Tomography technique images the changes in electrical resistivity of the subsurface. Resistivity is closely related to the presence of water, porosity, lithological characteristics, and permeability of materials (Luhn et al. 2023). The measurement consists of inducing a current in the subsoil by applying a voltage difference between two electrodes (called "current electrodes") and measuring the potential difference between two potential electrodes (Loke 2004). In this way, the resistivity distribution of the soil can be determined. In the case of a landslide, resistivity changes can allow identification of the slip surface, the zone of water accumulation, as well as the thickness of the different layers (Mreyen et al. 2021; Lapenna and Perrone 2022; Vivaldi et al. 2024).

In this case study, ERT measurements were conducted using an ABEM Terrameter LS acquisition system. The contact resistance was systematically measured before data acquisition to ensure good electrode-soil coupling. In all cases, the contact resistance was maintained well below the practical threshold of 3 kΩ, thus ensuring the accuracy and safety of the measurements, as well as the reliability of the resulting resistivity models. Data inversion was performed by means of the commercial software *ErtLab*^{TM} (Geostudi Astier S.r.l., Multi-Phase Technologies LLC - Sendrós et al. 2020; Balasco et al. 2022; Patrizi et al. 2022). The software allows to filter outliers data and to calculate the frequency distribution of several parameters, such as voltage, current intensity, geometric factor, and apparent resistivity. Then a statistical analysis is applied to exclude extreme values from the distribution tails. To further refine the results, Occam's regularisation is implemented (Santarato et al. 2011; Pazzi et al. 2018). *ErtLab*^{TM} allows the creation of a square cell mesh with a side equal to half the distance between the electrodes and a maximum depth calculated as a function of the largest quadripole used in the acquisition (Loke 2004). Moreover, *ErtLab*^{TM} allows the integration of a Digital Terrain Model, to better constrain the inversion procedure, taking into account not only the survey topography, but also the around space for an extension defined by the operator on the topography itself. This step is essential, especially in areas with significant relief, such as those in the study area, where neglecting topography would distort the subsurface resistivity image. All ERT datasets were inverted with a noise level of 1% and a constant noise value set to 0.0001. Specifically, the 1% relative noise level and the constant noise floor of 0.0001 are standard settings in *ErtLab*^{TM} to stabilise the inversion process and to prevent overfitting to noisy data. The addition of a small, controlled amount of noise helps the algorithm converge more reliably by assigning appropriate weights to data points during the Occam's inversion procedure Balasco et al. 2022; Santarato et al. 2011; Pazzi et al. 2018. For each 2D ERT, a starting homogeneous resistivity value of 20 Ωm was applied. This value was chosen based on the average resistivity value obtained from all the collected ERTs. Convergence was successfully achieved with a maximum of 9 iterations.

A total of 10 ERTs (4 for the Sérezé landslide, 3 for the Thimister landslide, and 3 for the Manaihan landslide) were collected using a Dipole-Dipole and a Gradient electrodes configuration (Dahlin and Zhou 2004). For each ERT, the apparent resistivity data were inverted both separately and jointly by combining the two arrays in order to have a more realistic model that takes into account the advantages and minimises the limitations of each array (Pazzi et al. 2020; Wei et al. 2024). In the "Results" section, only the outputs of the joint inversion will be presented.

Seismic refraction analysis

The Seismic Refraction Tomography technique is an active non-invasive seismic method: it uses a source (such a hammer) to generate underground vibrations that are recorded by geophones placed along the surface in a linear array. P-waves (compressional waves) and S-waves (shear waves) propagate at different speeds depending on the physical properties of the soil. The analysis of the first arrival times of P-waves recorded at each receiver allows the geometry of a layered subsurface and the propagation velocity of the seismic wave per layer to be defined (Chen et al. 2008; Ayolabi et al. 2009; Anomohanran 2013; Perrone et al. 2021).

In this case study, 9 SRTs (3 for each investigated landslide) were carried out on the landslides and near their crests. The array

configuration consisted of 48 vertical geophones connected to a 24-bit 48-channel DAQLinkII seismograph system of Georeva. The seismic energy was triggered by hammer shots on a nylon plate at several points along the profile Lines. Data were analysed using the Seisimager 2DTM software package developed by Geometrics (Dindar and Alevkayalı 2023). The Pickwin module was used to pick the first arrival times of the seismic waves, while the Plotrefa module was used for data inversion. The data were processed and inverted using the reciprocal time method, which enabled the creation of a tomographic inversion.

Multi-channel analysis of surface waves

The Multi-channel analysis of surface waves method is a geophysical technique used to determine a 1D shear wave velocity profile of a soil over depth using Rayleigh wave dispersion (Park et al. 1999). Rayleigh waves, characterised by low frequencies and high amplitudes (Zhang et al. 2023), travel along the free surface, i.e., the interface between soil and air, while their speed is related to the stiffness of the ground they cross. In stratified media, these waves exhibit dispersion, which means that their propagation speed varies with frequency (Foti 2005). Given the dispersion relation of the ground phase velocity, it is possible to calculate the Vs-wave velocity profile using the inversion method. Therefore, it is assumed that the Rayleigh wave velocity is approximately 0.9 times the Vs-wave velocity. This inversion method is well-suited in sub-horizontal terrain contexts marked by an increase in wave velocities with depth (Forchap and Schmid 1998). From the time series, with a record length of a few seconds, collected by a series of aligned geophones (thus multi-channel), a wavefield transform, e.g., f-k, can be used to create a full velocity spectrum in the frequency-phase velocity domain. Subsequently, f-k pairs that generally exhibit some spectral energy maxima are identified, and a Rayleigh wave dispersion curve is generated. Through an inversion process, by comparing experimental and theoretical dispersion curves, soil parameters such as layer thickness, shear wave velocity, and density are calculated, and 1D shear wave velocity profiles are generated over depth (Zhang et al. 2023).

In this work, the MASW analysis was carried out starting from the active seismic datasets that were recorded with vertical 4.5 Hz geophones, meaning that only the vertical components of Rayleigh waves are considered. For each SRT, it was possible to extract two 1D Vs profiles, one linked to the shot with an offset before the first geophone, and one for the shot with an offset after the last geophone. Dispersion curves were generated and picked with the linear f-k tool of Geopsy (www.geopsy.org, last access November 2024), while for the inversion, the dinver module of the Geopsy software was used (Wathelet et al. 2008). Note that the final result of MASW is a 1D Vs-profile over depth; the maximum possible depth of our inversion was hereby determined by one-third of the largest picked wavelength in the f-k spectrum.

H/V spectral ratio and H/V section reconstruction

H/V is a single-station passive seismic technique that calculates the ratio between the Fourier spectra of the horizontal and vertical components (Okada and Suto 2003) of the seismic noise (or microtremors) that is mainly made up of SH waves (Molnar et al. 2022), and must be acquired using three-component sensors. The H/V (or HVSR) method, initiated by Nakamura (1989) and further developed by, i.e. Ibs-von Seht and Wohlenberg (1999), allows to estimate the resonance frequency(ies) of a soil. In fact, this method provides H/V peak(s) at the resonance frequency(ies), that is(are) stable over time (Dal Moro and Panza 2022). The H/V peak frequency is related to the subsurface conditions, such as the contact between soft soil and a rocky substrate (Lotti et al. 2018): the higher the peak frequency, the shallower the interface depth. A flat H/V curve means no amplification and the absence of layers characterised by different properties. Thus, the higher the number of peaks, the higher the number of interfaces. Knowing the values of the Vs of the shallower layer, it is possible to obtain the depth of the interface corresponding to a given peak (Ibs-von Seht and Wohlenberg 1999; Castellaro 2016). In landslide studies, these H/V peaks can be related to the depth of the shear surface and the geometry of the landslide (Castellaro 2016; Pazzi et al. 2017; Mreyen et al. 2021; Song et al. 2021; Innocenti et al. 2023).

In this study, the measurements were performed with a Lennartz 3D/1 s seismometer connected to a CtySharkII microseismic station at a sampling frequency of 200 Hz. The acquisition lengths varied between 15 and 30 min. Data were processed using Geopsy software that implements the SESAME project guidelines (SESAME 2004; Dal Moro and Panza 2022). To obtain the spectra of the components, and thus the H/V ratio, each trace was analysed to keep the most stationary part of the signal, subdivided into non-overlapping windows of 20 s, smoothed by 40% of the central frequency wide (Konno and Ohmachi 1998) windows using a cosine taper with a width of 5%. Data were filtered using the STA/LTA ratio anti-triggering on the raw signal. In the "Results" section, only four representative measurements will be shown for each site, while the H/V section were reconstructed only for the Manaihan landslide using the same software as in Castellaro (2016) and will be presented in the "Discussion" section.

Results

In this section, the results of the geophysical investigations of each landslide will be presented, i.e., Sérezé landslide ("Sérezé landslide" section), Thimister landslide ("Thimister landslide" section), and Manaihan landslide ("Manaihan landslide" section).

Sérezé landslide

In total, four ERTs were collected to characterise the Sérezé landslide (SER-E1 to SER-E4, see Fig. 2). The surveys were principally located in the SE part of the slide to map its detachment scarp. The electrode spacing is variable for each profile and was adapted to enhance either lateral or vertical resolutions. The SER-ER1 has a profile length of 126 m with an electrode spacing of 2 m, while the SER-E4, in its prolongation, is 94.5 m long with a 1.5 m electrode spacing. SER-E2 (profile length 315 m) and the co-located SER-E3 (profile length 157 m) denote electrode spacings of 5 m and 2.5 m, respectively.

The measured resistivity values range from 5 to 50 Ωm. The SER-E2 survey (Fig. 2b) crosses the entire SE part of the landslide and shows a layer of low resistivity (<20 Ωm) 10 to 20 m below the surface in the middle to lower portion of the slope. This result is comparable with the electrical resistivity study performed by Demoulin et al. (2003). The co-located survey SER-E3 of higher

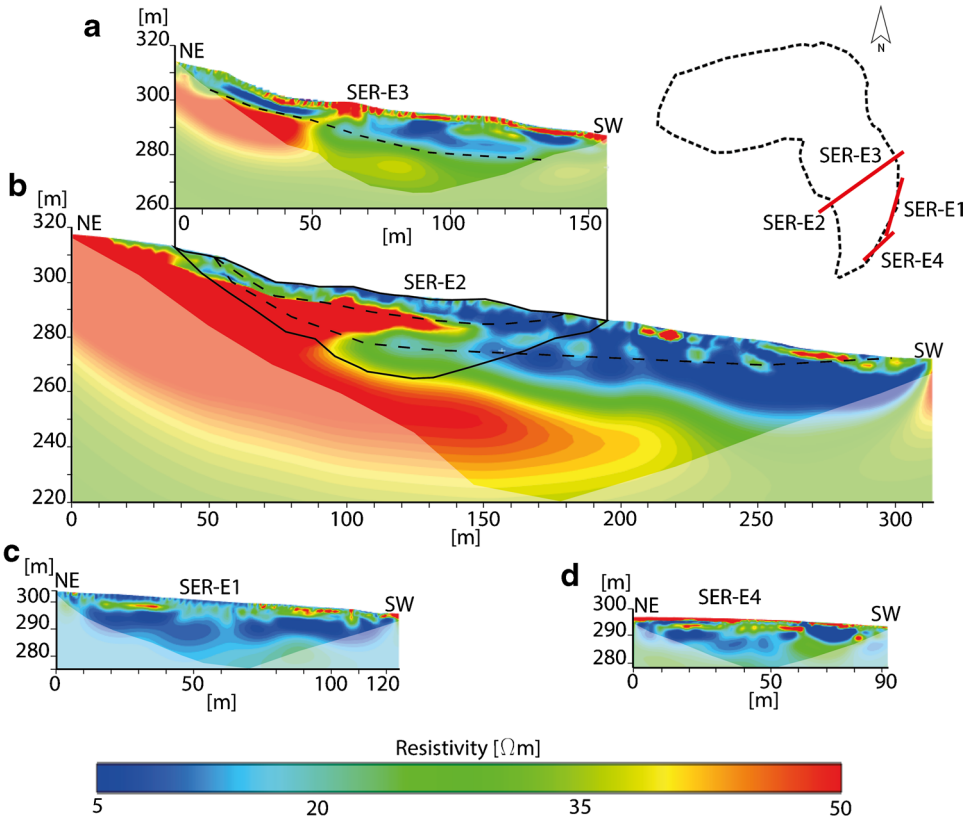

Fig. 2 Electrical resistivity tomographies at the Sérezé landslide: the whitened areas represent areas with a higher model uncertainty. **a**, **b**, **c**, and **d** respectively represent the sections SER-E3, SER-E2, SER-E1, and SER-E4; the black line in **b** marks the borders of SER-E3 shown in **a**. The black dashed lines in **a** and **b** indicate the likely existence of a double sliding surface. The map in the upper right corner shows the location of ERTs surveys

resolution reveals the same 10 to 20 m superficial layer of low resistivity values (Fig. 2a). For the SER-E4 survey (Fig. 2d), a greater variation of resistivity values can be seen in the surface portion. The superficial layers of low resistivity in SER-E2 and SER-E3 probably mark the landslide mass and its shearing horizon located at a depth of 10 to 20 m, with increasing landslide thickness towards SW at the toe (see the black dotted line in Fig. 2a and b). The likely existence of a double sliding surface explains the higher resistivities observed in SER-E2 at intermediate depths (10 m). In contrast, the right part of SER-E2 shows low resistivities, which can be attributed to the presence of shales. The boundary of the landslide material is marked by a line of small higher-resistivity blocks, visible as small green zones (Fig. 2b.

Three P-wave seismic refraction surveys were performed at the Sérezé landslide (SER-S1 to SER-S3, Fig. 3), more or less in co-location with the ERTs presented before. The SRT results are shown in Fig. 3a–c and display P-wave velocities ranging from 250 to 2500 m/s. The SER-S1 (Fig. 3a) crosses the south-eastern part of the landslide body from NE to SW and reveals a lateral increase in P-wave velocity at approximately 50 to 100 m of the profile length; in the NE half of the profile, V_P >2000 m/s are reached at 40 m depth, while in the SW part of the profile, these velocities are reached at a shallower depth of 20 to 25 m. SER-S2 (Fig. 3b), located east of the landslide border, shows a homogeneous subsurface in terms of P-wave velocities, with V_P reaching 2500 m/s at 30 m depth. In prolongation of the latter, SER-S3 (Fig. 3c) is marked by a lateral contrast in V_P at 65 m of the profile length, with higher V_P at the SW part than in the NE part of the profile at 10 to 20 m depth.

As described in the "Materials and methods" section, the MASW analysis was performed from the active seismic data, and two 1D velocity profiles were extracted for each dataset. The results of this analysis for the Sérezé landslide are shown in Fig. 3h–j. Profiles S1-NE, S2-SW, and S3-SW, acquired at the landslide boundary, show similar values, with a Vs change at the same depth (22, 27, and 24 m respectively) with a velocity of 600 m/s, except for profile S2-SW, which rises to 1000 m/s. The S1-SW profile, the only one within the landslide body, shows a transition to higher velocities (600 m/s) as early as 13 m deep, showing either a shallow sedimentary cover or an approach of the shear horizon to the surface. The S1-SW and S2-NE (Fig. 3h, i) profiles reveal the presence of another very shallow layer, with a thickness between 3 and 5 m and shear wave velocities of less than 200 m/s. This layer could be associated with the peak identified by SER-072 (Fig. 3d), which indicates a horizon of approximately 5 m deep.

The H/V analysis in Sérezé landslide identifies clear frequency peaks in the range of 2 to 4 Hz, with amplitudes of 6 or greater

(four selected measures are shown in Fig. 3d–g, and their location is indicated in the upper right corner of Fig. 3). The SER-067 measure (Fig. 3e) is located north of the landslide border at 315 m a.s.l. and shows the lowest frequency f_0 at 2.0 Hz. In addition, the measures within the landslide area, located at lower altitudes, present peaks around the same low frequency. However, it is possible to observe secondary peaks of very low amplitude for these measurements in the frequency range of 12 to 15 Hz. In addition, the SER-072 measurement (Fig. 3d) is marked by a larger fundamental peak (covering frequencies of 3–6 Hz).

Thimister landslide

To characterise the Thimister landslide, three ERTs were located in correspondence with the detachment scarp, that is, the southern-western border (Fig. 4). THI-E1 is oriented parallel to the scarp and covers 315 m with electrodes spaced by 5 m. THI-E2 and THI-E3 (length 157.5 m, electrode spacing 2.5 m) cross the latter nearly perpendicularly and are marked by a pronounced topography as they map the landslide scarp. THI-E1 (Fig. 4a) shows a horizontal stratification of the layers. The surface is characterised by high resistivity values (50 Ωm) and below this there is an alternation between a more conductive material (5–10 Ωm approximately 5 m above ground level) followed by slightly more resistive material (20 Ωm approximately 10 m above ground level). THI-E2 (Fig. 4b) presents the same shallow layer of higher resistivity values and is marked by lateral contrasts at the top and bottom of the detachment scarp. Similar contrasts, with low resistivity zones bent, can be found in THI-E3 (Fig. 4c).

The horizontal layers detected in THI-E1 most likely correspond to lithological contacts, such as a more resistive superficial layer of Gulpen chalk on top and low resistivity Vaals clays possibly underlain by Aachen Sands (or even Carboniferous bedrock) at depth. However, the vertical structures in THI-E2 and THI-E3 seem to be related to mass movement phenomena, where low resistivity layers possibly mark shearing horizons of a reactivation of the landslide. Both profiles indicate a rotational movement of the mass due to the rounded shape of the contrasts.

In total, three SRTs, collocated with ERTs, were acquired at the detachment scarp: the results are shown in Fig. 5. THI-S1 and THI-S3 (Fig. 5c and a, respectively) cross the landslide scarp and are marked by their pronounced topography. Both SRTs present a 15 m thick layer of relatively low velocities (<1000 m/s) in the upper part of the scarp and behind it, which is reduced to a few meters at the bottom of the slope. With further depth, the surveys show a rather homogeneous increase in P-wave velocity up to >2500 m/s in approximately 50 m below the surface. The profile parallel to the detachment scarp, THI-S2 (Fig. 5b), shows the same low-velocity layer in the first 15 m. A small lateral change in the velocities of the P-wave is present at 30 to 40 m profile length and reveals a shift in velocities over 15 m; the maximum V_P reached by this survey is 2000 m/s.

The results of the MASW analysis performed on the SRT data are shown in Fig. 5h–j. All profiles are in accordance with the SRT, identifying a shallower layer characterised by an S-wave velocity of about 250 m/s and a thickness of a few meters up to ~15 m, and a deeper layer characterised by an S-wave velocity of about 400–600 m/s. Four of the H/V results of the Thimister landslide are shown in Fig. 5d–g. They indicate fundamental frequency peaks in the range of ~2 to 5 Hz with amplitudes higher than 6. Measures within the scarp area, THI-187 and THI-189 (Fig. 5d and f), show frequency peaks at 1.8 Hz and 1.9 Hz, respectively. The recorded data are marked by elevated noise at frequencies <1 Hz, which is not considered here due to the eigenfrequency of 1 Hz of the used seismometer. Similarly to the Sérezé HVSR results, the measurement THI-153 (Fig. 5b) reveals a secondary frequency peak at 12 Hz (amplitude of 2).

Manaihan landslide

In the Manaihan landslide, three ERTs (MAN-E1, MAN-E2, and MAN-E3, Fig. 6) were carried out to identify the electrical properties of the materials affected by movement and the areas of accumulation of water along the slope. MAN-E1 (Fig. 6a), NE-SW oriented, is 372 m long (electrode spacing of 3 m) and crosses the landslide from the crown to the toe. MAN-E2 (254 m long, with an electrode spacing of 2 m, Fig. 6b) is W-E oriented and crosses MAN-E1 almost in its central portion. MAN-E3 (252 m long, electrode spacing of 2 m, Fig. 6c) is SW-NE oriented, crosses the landslide crown, and reaches almost the landslide toe near MAN-E1. The highest resistivity values (80–100 Ωm; note, here the colour scale was set to the maximum value of 50 Ωm) are recorded in MAN-E1 and MAN-E3 scarp zone and 10 m below the surface, starting from the central portion of the three ERTs up to the end. In all sections, a more conductive zone with values between 10 and 40 Ωm is present up to 20 m depth from the scarp to the central/final portion of the ERTs, reaching 5 m in depth. A good agreement in the resistivity values can be observed at the intersections between MAN-E1 and MAN-E2 and between MAN-E1 and MAN-E3. From a geological point of view (Fig. 1), the layer with the highest resistivity can be traced by the geological map to the Vaals clays - Aachen sands and the layer with the lowest resistivity to the Houiller shales.

Figures 7a–c show the results of the P-wave SRTs MAN-S1, MAN-S2, and MAN-S3, respectively. MAN-S1 (Fig. 7a) crosses the landslide scarp in the northern landslide half in a NW-SE direction (profile length 141 m). MAN-S2 (Fig. 7b) is situated in the central-southern part of the slide in a SSW-NNE orientation with a profile length of 235 m (geophones 5 m spaced), while the co-located MAN-S3 (Fig. 7c) can be considered higher resolution zoom of the last portion of MAN-S2 as it was placed at the central point of MAN-S2 with a shortened geophone spacing of 3 m. The results of the seismic refraction model show the presence of two main layers: one shallower with P-wave velocities ranging between 500 and 800 m/s, and one deeper characterised by P-wave velocities between 1500 and 2800 m/s. The thickness of the first layer is more pronounced near the scarp and outside the landslide (about 20 m), while lower thicknesses are present at the landslide toe (5 m for section MAN-S1 and 2–3 m for sections MAN-S2 and MAN-S3).

The results of the MASW analysis performed on the SRT data are shown in Fig. 7h–j. They are in agreement with the SRT results. The two profiles acquired outside the landslide (S1-NW in Fig. 7h and i) identify a superficial layer of about 10 m characterised by a S-wave velocity of ~200 m/s, while those acquired within the landslide (S1-SE in Fig. 7h and j) show a shallower layer characterised by a thickness of ~5 m and a shear waves velocity of ~100 m/s. Only the MASW from MAN-S2 reaches a depth higher than 10 m and

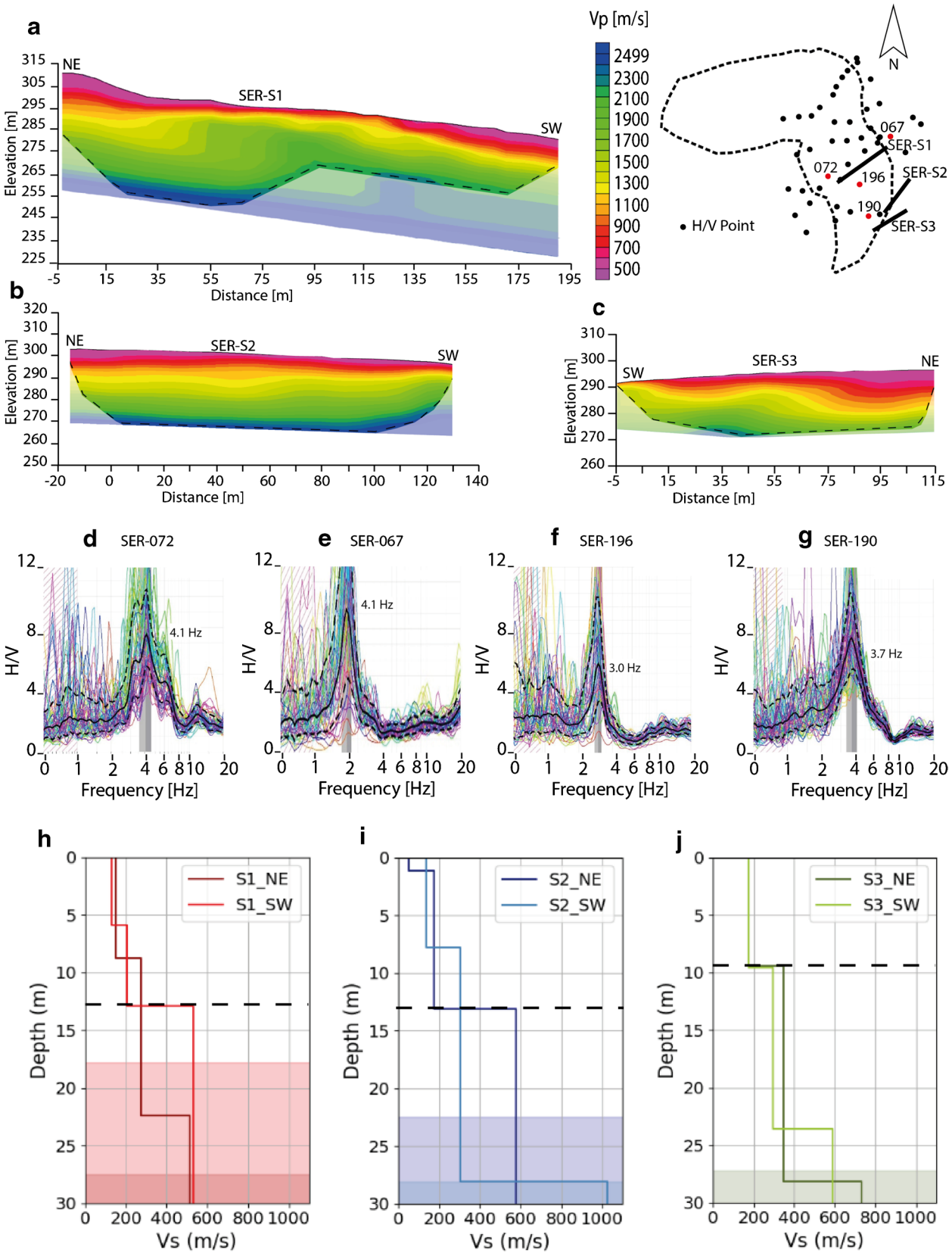
a
NE
SER-S1
SW
Elevation [m]
Distance [m]
Vp [m/s]
2499
2300
2100
1900
1700
1500
1300
1100
900
700
500
N
067
SER-S1
072
196
SER-S2
190
SER-S3
H/V Point
b
NE
SER-S2
SW
Elevation [m]
Distance [m]
c
SW
SER-S3
NE
Elevation [m]
Distance [m]
d SER-072
4.1 Hz
e SER-067
4.1 Hz
f SER-196
3.0 Hz
g SER-190
3.7 Hz
H/V
Frequency [Hz]
h
S1_NE
S1_SW
i
S2_NE
S2_SW
j
S3_NE
S3_SW
Depth (m)
Vs (m/s)

◂**Fig. 3** Seismic survey results of the Sérezé landslide. The map in the upper right corner shows as lines the location of SRTs surveys and as dots the H/V acquisitions. **a**, **b**, and **c** Seismic refraction tomographies (SRT): SER-S1, SER-S2, and SER-S3, respectively. The black dashed lines, together with the whitened areas, show the outer limits of the beam paths used for tomographic inversions. **d**, **e**, **f**, and **g** H/V curves: SER-072, SER-067, SER-196, and SER-190, respectively, marked in red in the map in the upper right corner. The fundamental frequency peaks are marked by the grey bars. **h**, **i**, and **j** 1D velocity profiles from MASW analysis of SER-S1, SER-S2, and SER-S3, respectively. Each sub-plot shows the 1D velocity profiles obtained by the bidirectional shots with offsets before the first (NE direction) and after the last (SW direction) geophones. The colored areas indicate subsoil depth affected by a higher model uncertainty. Dashed lines mark the basis of landslide with Vs ≤200 m/s

identifies a layer, below this depth, characterised by an S-wave velocity of about 400 m/s.

The H/V curves on the Manaihan landslide show frequency peaks in the range between 2 and 5 Hz with amplitudes around 10 (Fig. 7d–g). The MAN-148 measurement (Fig. 7d) is located NW MAN-S1, outside the landslide, and shows a fundamental frequency of 2.3 Hz. Measurements taken within the landslide show higher frequency values, significant for a shallower contrast. MAN-182 and MAN-183 (Fig. 7g and f, respectively) were carried out near the slope at a lower altitude than MAN-148. Probably, the peaks are affected by the topographic variation and are therefore indicative of the different thicknesses in the investigated area of the Vaals clays mixed with Aachen sands and underlying Houiller shales. MAN-171 (Fig. 7e) was carried out near a surface runoff and in an area of the body of the landslide characterised by depressions and swellings Linked to movement. Therefore, this measurement may represent a variation of the shear surface along the landslide area, which tends to become shallower toward the toe. From the analysis of the MASW results, it was observed that the western, central, and eastern portions of the Manaihan landslide were characterised by three different surface S-wave velocities: 180 m/s, 170 m/s, and 140 m/s, respectively. These values were used to obtain the H/V sections.

Discussion

The geology of the *Pays de Herve* and the related literature (Demoulin 1988; Demanet 2000; Demoulin et al. 2004) identify two main formations that belong to Cretaceous deposits resting in a Paleozoic basement. At the base, there is the Aachen formation, consisting of fine sands intercalated with coarse sands and clays, with a thickness up to 10 m in the eastern part of the target area, while the sands are almost disappearing in the western part. Above it lies the Vaals formation, consisting of clays and marls, with a maximum thickness

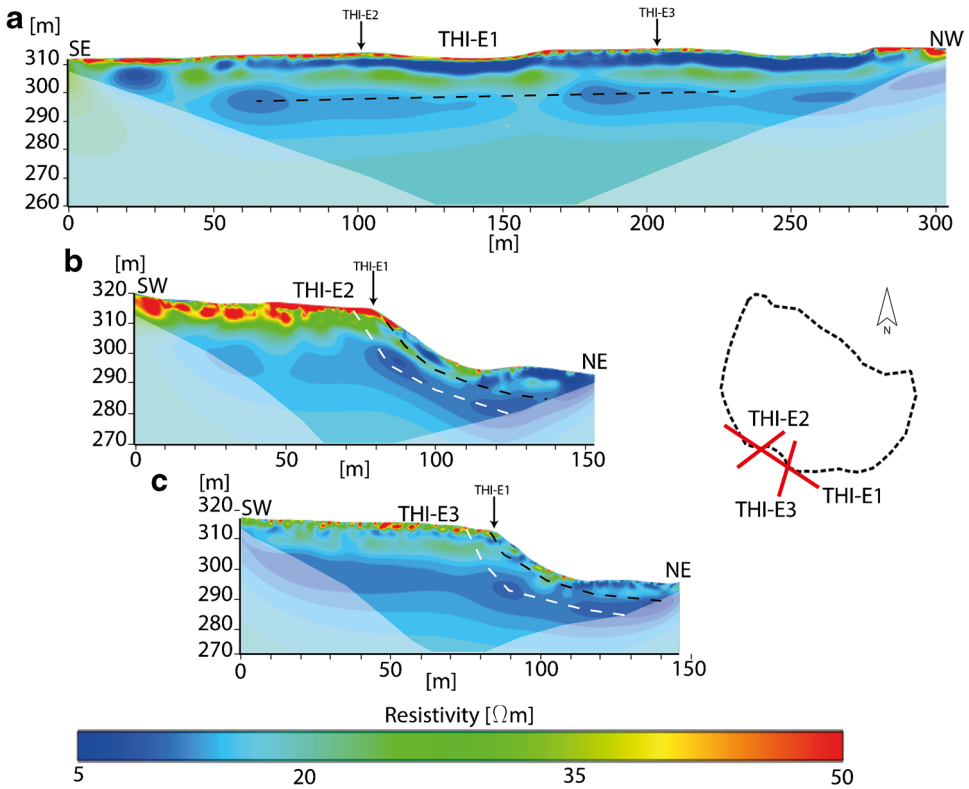

Fig. 4 Electrical resistivity tomographies at the Thimister landslide: the whitened areas represent areas with a higher model uncertainty. **a**, **b**, and **c** respectively represent the sections THI-E1, THI-E2, and THI-E3. The map at the center shows the location of ERT surveys. The black arrows indicate the point of intersection between the sections. The dashed black lines highlight the probable sliding horizons. The dashed white line marks the horizon of the existing, but not fully developed landslide surface that may be capable of producing a new landslide in the future

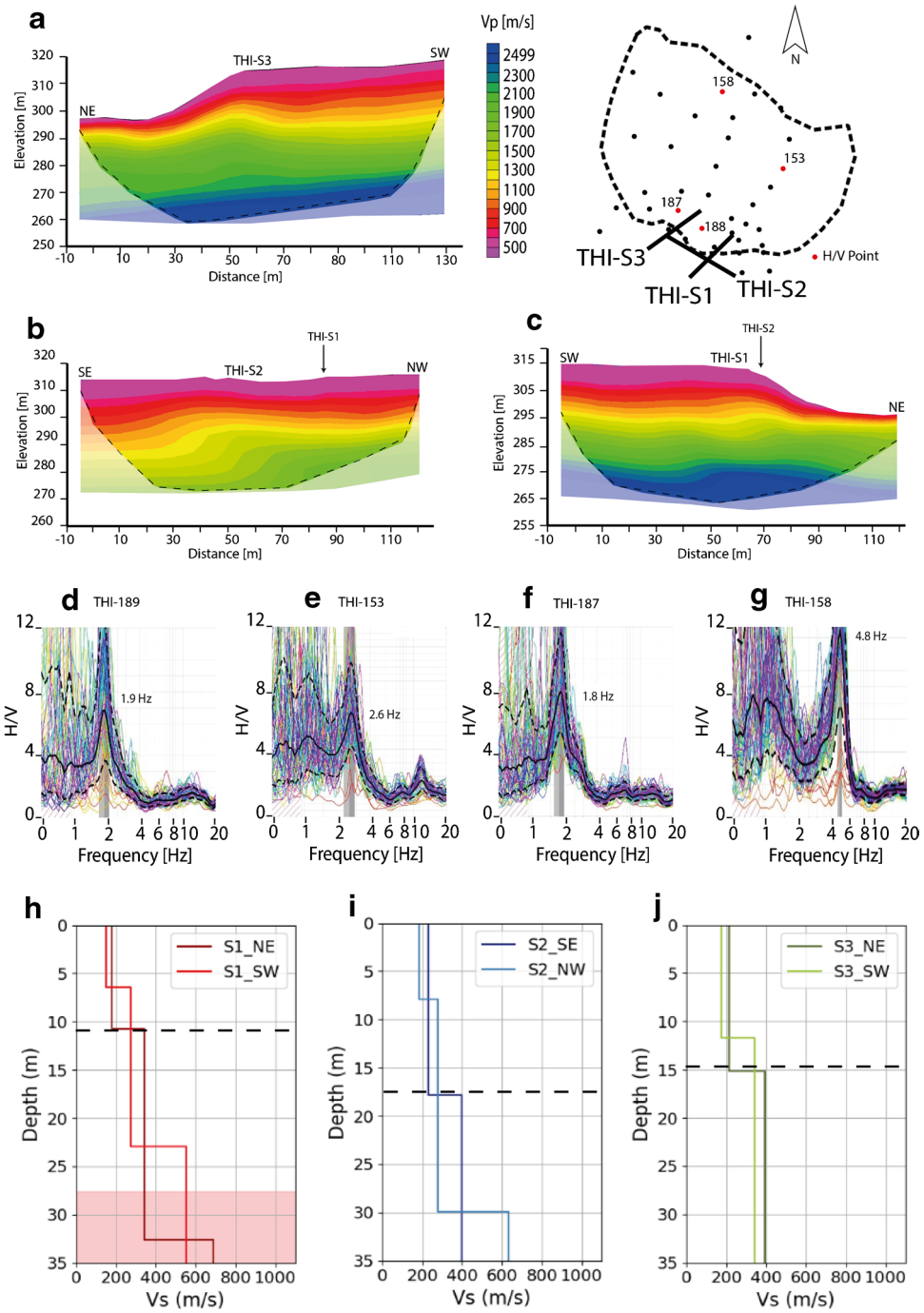

Fig. 5 Seismic survey results of the Thimister landslide. The map in the upper right corner shows as lines the location of SRTs surveys and as dots the H/V acquisitions. **a**, **b**, and **c** Seismic refraction tomographies (SRT): THI-S1, THI-S2, and THI-S3, respectively. The black dashed lines, together with the whitened areas, show the outer limits of the beam paths used for tomographic inversions. The black arrows indicate the point of intersection between the sections. **d**, **e**, **f**, and **g** H/V curves: THI-189, THI-153, THI-187, and THI-158, respectively, marked in red in the map in the upper right corner. The fundamental frequency peaks are marked by the grey bars. **h**, **i**, and **j** 1D velocity profiles from MASW analysis of THI-S1, THI-S2, and THI-S3, respectively. Each sub-plot shows the 1D velocity profiles obtained by the bidirectional shots with offsets before the first and after the last geophones. The coloured areas indicate subsoil depth affected by a higher model uncertainty. Dashed black lines mark the basis of landslide with Vs ≤400 m/s

of 30 m in the study area. The geophysical surveys carried out to characterise the three *Pays de Herve* landslides, and presented in the "Results" section, could confirm, in the study area, the thickness estimated by Demoulin et al. (2003) for the upper geological formations.

The H/V surveys on the Manaihan landslide showed frequency values between 2 and 4 Hz in its upper part and relatively higher frequency values near the toe of the landslide and its margins. The higher frequency values could represent a lower depth

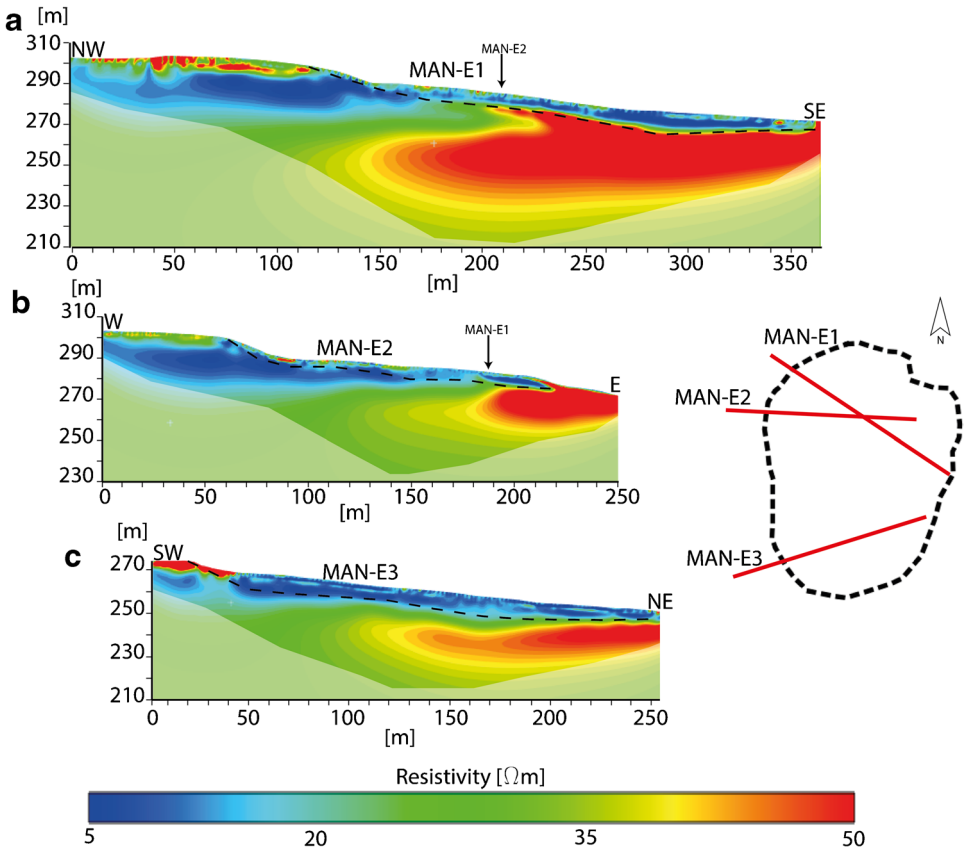

Fig. 6 Electrical resistivity tomographies at the Manaihan landslide: the whitened areas represent areas with a higher model uncertainty. **a**, **b**, and **c** respectively represent the sections MAN-E1, MAN-E2, and MAN-E3. The map in the central portion shows the location of ERT surveys. The black arrows indicate the point of intersection between the sections. The dashed black lines highlight the probable sliding horizons

contrast between the two main identified layers, indicating a less pronounced deepening of the interface. Thus, data suggest a difference, within the landslide, in the thickness of the two main layers. These variation is also identified by electrical and seismic tomographies. H/V surveys show variable thickness of 23–24 m for the MAN-148 and 13 m for the MAN-171 measurement and reach values of 5 m at the foot (Fig. 7). The ERT surveys reveal the presence of two layers: one primarily conductive, with resistivity values ranging between 5 and 20 Ωm, which is deeper near the landslide crown and thins out towards the toe. The second, more resistive layer, has values between 35 and 50 Ωm. This is consistent with the seismic tomographies, which also show two layers. The first, with P-wave velocities between ~500 m/s, also due to the presence of water and ~800 m/s, exhibits the same behaviour as the conductive layer, thinning toward the toe. The second layer, which is shallower on the toe, shows higher velocities that exceed ~ 1500 m/s. Observing the seismic and electrical tomographies (Figs. 6 and 7), a concordance can be noted in identifying two sub-horizontal layers and, consequently, the presence of an interface at a variable depth between 10 and 30 m. However, considering all the geophysical surveys and their locations, it is evident that this interface is present along the entire length of the profiles, including outside the landslide body. This suggests that the surveys have identified a lithological contact, probably that between the Vaals clays - Aachen sands and the Houiller shales. Because there are no significant anomalies in the ERT and SRT tomographies nor inversions in seismic wave velocities, it can be assumed that the shear surface coincides with the lithological contact.

Everything indicated until now is certainly valid for the areas near the ERTs and SRTs sections, but is it possible to extend this conclusion to the entire landslide(s)? The H/V seismic noise acquisitions, and in particular their representation as H/V sections (i.e., H/V contour plot of the acquisitions along a transect and converted into the H/V-depth domain from the H/V-frequency one, Castellaro (2016)), can help in answering this question. Among the three landslides, the Manaihan landslide was chosen as an example to show how H/V sections can help to obtain a 3D view, and thus extend the conclusion to the whole landslide. As mentioned in the "Introduction" section, the hypothesis to reconstruct H/V sections is the presence of sub-horizontal layers and an increase in velocities with depth, and in the literature, there are many examples of landslides H/V sections (Castellaro 2016; Pazzi et al. 2017; Song et al. 2021; Seitone et al. 2025). Moreover, as said in Ibs-von Seht and Wohlenberg (1999) and Delgado et al. (2000), the thickness of a resonant layer and its resonant frequency are linked to the

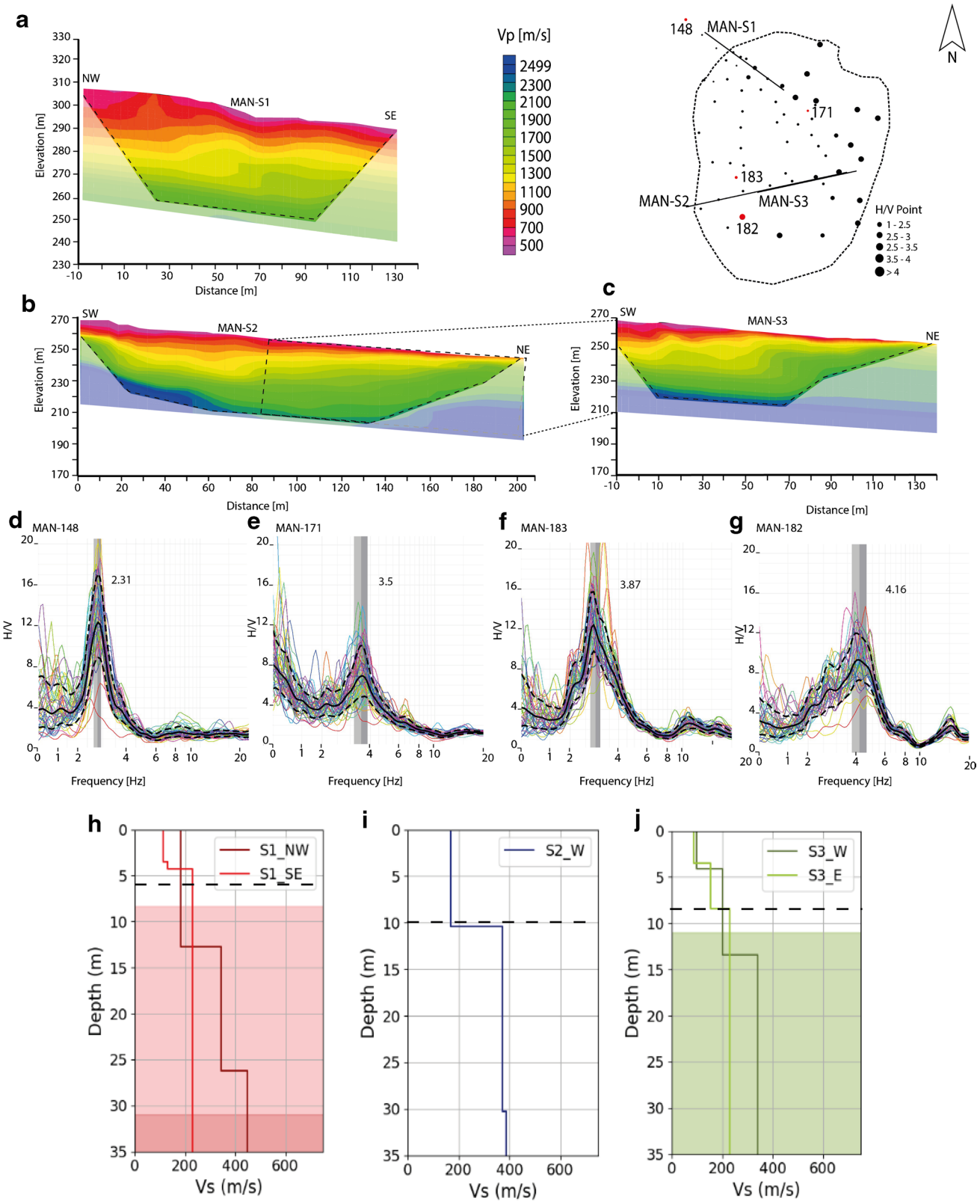

surface S-wave velocity using a power-law regression model. Using the tool developed by (Castellaro 2016), the three different surface S-wave velocities (180 m/s, 170 m/s, and 140 m/s) obtained from the MASW were used to obtain the H/V sections in the three different sectors of the Manaihan landslide. For the H/V sections crossing more than one sector, an average value of 170 m/s was used. Three

◂**Fig. 7** Seismic survey results of the Manaihan landslide. The map in the upper right corner shows the locations of SRTs surveys as lines and as the H/V acquisitions as dots. **a**, **b**, and **c** Seismic refraction tomographies (SRT): MAN-S1, MAN-S2, and MAN-S3, respectively. The black dashed lines, together with the whitened areas, show the outer limits of the beam paths used for tomographic inversions. **d**, **e**, **f**, and **g** H/V curves: MAN-148, MAN-171, MAN-183, and MAN-182, respectively, marked in red in the map in the upper right corner. The fundamental frequency peaks are marked by grey bars. **h**, **i**, and **j** 1D velocity profiles from MASW analysis of MAN-S1, MAN-S2, and MAN-S3, respectively. Each sub-plot shows the 1D velocity profiles obtained by the bidirectional shots with offsets before the first (NW or SW direction) and after the last (SE or NE direction) geophonevs. The coloured areas indicate subsoil depth affected by a higher model uncertainty. Dashed lines mark the basis of landslide with Vs ≤ 200 m/s

representative H/V sections aligned along the ERTs profiles MAN-E1, MAN-E2, and MAN-E3 were obtained, and they are shown in Fig. 8a–c. Figure 8d and e show a 3D EW-view of the three sections as well as a common view of all sections. These sections are shown in terms of amplitude.

Comparing MAN-H/V1 - MAN-H/V3 (Fig. 8a–c) with the ERTs and SRTs results (Figs. 6a–c and 7a–c, respectively), a similar pattern of contrasts was observed between layers. The main H/V contrast, characterised by the maxima of the H/V amplitudes (between the range 10–25, i.e., yellow to orange corresponding to frequency values lower than 2 Hz), is located at a depth that varies between ~15 and ~40 m (the dashed-dotted red line in Fig. 7a–c), and it is possible to note that this interface is present in the whole landslide and also outside its boundaries (here with the highest amplitude). Given the depth of the interface, it suggests that it could be caused by the interface between the soft deposits (sub-horizontal Vaals and Aachen layers) and the folded Paleozoic basement. Starting more or less from the surface, up to the depth of that varies between ~10 and ~20 m, the whole landslide is characterised by very low H/V amplitude values (dark blue colours). It can be related to the low resistive layer highlighted in the ERTs (Fig. 6a–c). Despite the quite high uncertainty linked to the H/V sections method (i.e., using surface S-wave velocity values that differ by a few tens of m/s cause a variation of a few meters in the final model), from the analysis of all the Manaihan Landslide H/V sections it is possible to assess that the slip surface corresponds to the lithological contact between the mixture of Vaals and Aachen layers and the Houiller shales (dashed red line in Fig. 8).

The geophysical data of the Manaihan landslide are in agreement with the geognostic data described by Demoulin and Glade (2004). In particular, in their paper, the authors demonstrate that the penetrometric surveys (CPT) showed a clear variation in penetration resistance that allows a distinction between the landslide mass and the underlying rigid substrate. In the upper part of the slope, this contact is between 6.0 and 10.0 m deep, while further downstream, a more superficial limit was observed, around 2.5–3.8 m. These observations are consistent with the deformations measured by the inclinometers. The device installed at the top of the slope recorded a progressive displacement with a sliding surface located around 5.5–6.0 m, in correspondence with the transition to the substrate identified by the CPT measurements. In contrast, the inclinometer installed in the lowest part of the slope showed a rapid deformation at a depth of only 2.5 m, suggesting a different behaviour of the landslide body, probably related to a shallower sliding surface near the landslide foot. These results reinforce the interpretation of the internal structure of the slope, confirming the existence of well-defined shear surfaces that separate loose or remobilised materials from more resistant substrates. This is also confirmed by the trench results reported in Demoulin et al. (2003) for the Sérezé and Thimister landslides. The authors state that all trenches revealed the presence of large, undulating shear surfaces, and in one of them, blocks of stratified Aachen sands interlayered with clay were found. These observations indicate that the movement developed at the contact between these sandy-clayey soils and the Palaeozoic basement.

Figure 8d (MAN-H/V4 section) overlays the H/V section with the geotechnical data (CPTs and inclinometers) from Demoulin and Glade (2004): the inclinometer rupture depths (white circles), the maximum landslide depth from CPTs (white solid line), the interface between the landslide mass and progressively less-weathered bedrock (white dashed line), and the potential surface of the undisturbed valley (white dotted line). The red dashed line represents the contact between the Vaals clay - Aachen sands complex and the Houiller shales, as supposed by the H/V data interpretation. The red dashed line represents the contact between the Vaals clay - Aachen sands complex and the Houiller shales, as supposed by the H/V data interpretation. Geophysical and geotechnical data agree in highlighting the contact between the Vaals clay and the Aachen sands mix with the underlying shales. Moreover, as reported by Demoulin and Glade (2004), the CPT data alone are not sufficient to fully demonstrate the development of the movement.

The geophysical data collected for the Manaihan landslide were integrated into a 3D geomodel of the slope in its current state (Fig. 9a–c). Ambient noise measurements (H/V) were incorporated into the geomodel as vertical logs (Fig. 9d–f) (Mreyen et al. 2021). Using the same S-wave velocity values employed to reconstruct the H/V sections, the H/V measurements help identify seismic impedance contrasts within the subsurface. In particular, a contrast was detected and interpreted as that between soft deposits and Upper Carboniferous shales (pink plane in Fig. 9). As can be seen in Fig. 9d–f, the contrast between the two materials obtained from the H/V amplitude agrees well with the ERT and SRT data. The modeled H/V amplitude thus illustrates the thickness of the identified subsurface units and is used to model geological interfaces (Fig. 9d–f) and volumes (Fig. 9g–h).

In accordance with what was observed for the Manahian landslide, similar findings are also noted for the Sérezé landslide and Thimister landslide. These results are summarised in Table 1. At the Sérezé landslide, the fundamental frequency of the H/V curves seems to vary according to the topography, and it is likely to be indicative of the thickness of the sub-horizontal Vaals and Aachen layers that increases with altitude. With an S-wave velocity of 250 m/s for the shallow upper Cretaceous layers, estimated by MASW analysis, the altitude of the basis of the combined Vaals and Aachen layers is estimated at approximately 275 m a.s.l. for all four H/V measurements (layer thickness varying between ~15 and 30 m). However, the S1-SW profile (Fig. 3h) shows that within the

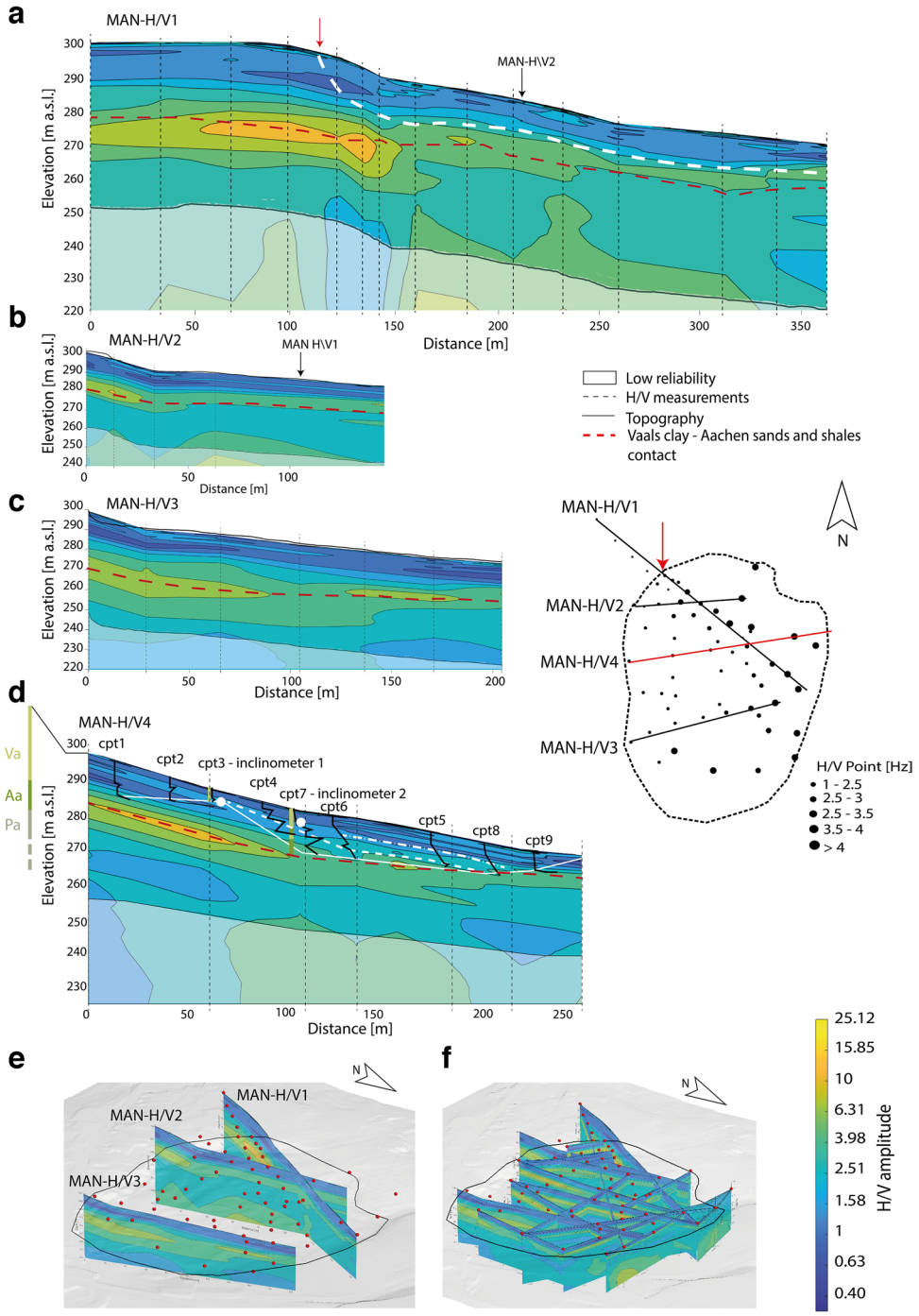

Fig. 8 Contour plot of the H/V curves acquired following the alignments of the H/V measurements and converted from the H/V-frequency to the H/V-depth domain. The colour scale indicates the H/V amplitude. **a**, **b**, and **c** three H/V sections created in correspondence of the MAN-ERT measurements. **d** H/V section, oriented according to the CPTs and inclinometers alignment (see red line for position) as reported in Demoulin and Glade (2004), over layered with CPTs and inclinometers data (modified from Demoulin and Glade (2004)). On the left of the MAN-H/V4 section, the light green bar labelled with Va refers to the Vaals clay, the dark green bar (Aa) to the Aachen sands, and the grey bar (Pa) to the underlying shales. In all the panels, the dashed black lines represent the location of the H/V measurements, while the whitened areas indicate a higher model uncertainty. The red arrow in **a** indicates where the H/V section passes through the landslide crown. **e** intersection between the MAN-H/V1 and MAN-H/V2 sections. **f** all the sections created by means of the H/V measurements. The dashed red line represents the contact between the Vaals clay - Aachen sands mix and the Houiller shales. The white dashed line in **a** outlines the basis of the landslide located in lithological contact between soft deposit and Houiller shales

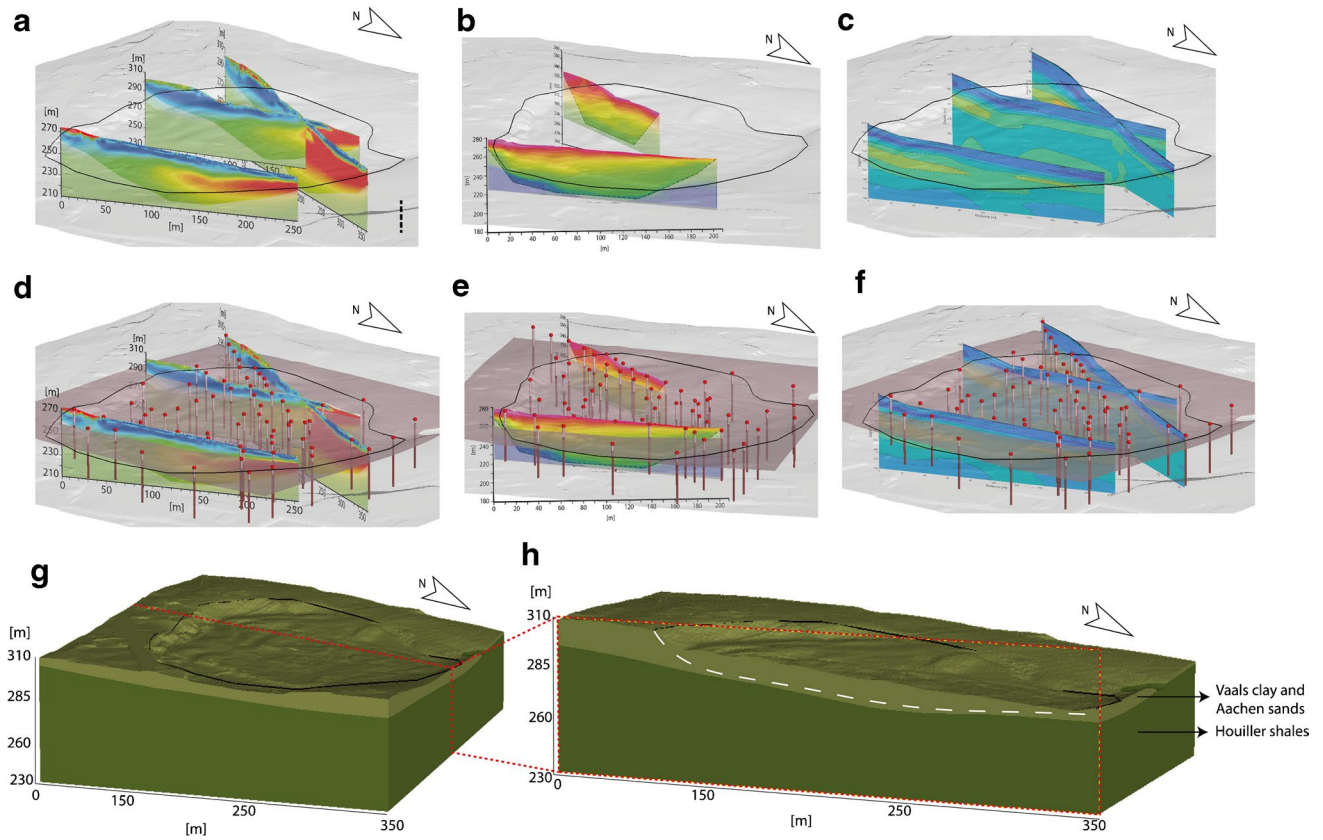

Fig. 9 Geomodel construction of the Manaihan slope with modelling and insertion of 2D geophysical profiles. **a**, **b**, and **c** ERT, SRT, and H/V sections in 3D. **d**, **e**, and **f**. The same sections with the integrated H/V logs and the contrast plane (pink) between the two materials identified by the acoustic impedance peaks. **g** and **h** the volumes, i.e., Vaals clay - Aachen sands mix and Houiller shales. The dashed red line represents the vertical cutting plane represented in h by the dashed red rectangle. The dashed white line represents the possible sliding surface

body of the landslide, there is a more superficial change of velocity (at 13 m depth), suggesting the possibility of a thinner cover or a shallower shearing horizon. The same change is highlighted by the H/V measurements. Small secondary peaks at higher frequencies, such as the 12 Hz peak in SER-072, would indicate a horizon located at a depth of 5 Hz m (cf. Fig. 3d).

The small bumps in the SRT results of THI-S3 and THI-S1 could be of the same origin as the lateral resistivity changes present in THI-E2 and THI-E3, respectively. For all three surveys THI-S1 - THI-S3, it is possible to note a 10 to 15 m thick surface layer of low velocities that confirms the low elastic properties of the weak upper Cretaceous subsurface present in the study area.

Table 1 Landslide characteristics including resistivity (ρ), *P*-wave velocity (V_p), shear wave velocity (V_s), the interface mean fundamental frequency (f_{0mean}), and interface depth

Landslide	Layer 1	Layer 2	Interface f_{0mean}	Interface Depth
	ρ = 30–50 Ωm	ρ = 5–20 Ωm		
Sérezé	V_p = 500–1000 m/s	V_p = >2000 m/s	3.5 Hz	10 m
	V_s = 200 m/s	V_s = 600 m/s		
	ρ = 50 Ωm	ρ = 5–10 Ωm		
Thimister	V_p = <1000 m/s	V_p = >2500 m/s	2.5 Hz	10–15 m
	V_s = 200 m/s	V_s = 600 m/s		
	ρ = 80–100 Ωm	ρ = 10–40 Ωm		
Manaihan	V_p = 500–800 m/s	V_p = 1500–2800 m/s	3 Hz	5–10 m
	V_s = 200 m/s	V_s = 400 m/s		

Considering a S-wave velocity of ~250 m/s for the Upper Cretaceous sediments, it is possible to situate a contact layer at 265 m a.s.l., i.e., impedance contrast ~15 to 35 m below surface (e.g., the 2.6 Hz peak in THU-153). Again, it is possible to suppose that this contrast is caused by the lithological contact, which possibly also could have served as the basal shearing horizon of the slide. The Thimister landslide reaches a larger depth than the Sérezé landslide and shows slightly higher Vs values. The slide material has not been recently reactivated in contrast to Sérezé that can be considered an active landslide. The deeper sliding surface, marked by the white dashed line in Fig. 4, could cause future reactivations of the landslide. The Manaihan landslide appears to be the shallowest, as it shows H/V values mostly above 2 Hz, while for the other two landslides, particularly the Thimister landslide, H/V values slightly below 2 Hz were recorded, indicating a slightly deeper movement.

Conclusions

The widespread slope instabilities in the *Pays de Herve* (Belgium) region are related to the presence of soft layers of sand-silts, clays, and marls. Most failures occur within the clays or the mixture of clays and sands at the basis of these layers; failures can be triggered or reactivated by a combination of climatic and seismic events. To show the advantages of geophysical methods in characterising these phenomena and their help in reconstructing 3D geological models, three representative landslides in the *Pays de Herve* area were selected: the Sérezé landslide, the Thimister landslide, and the Manaihan landslide. They were characterised by means of ERTs, P-wave SRTs, MASW, and H/V measurements. The first three techniques allowed us to characterise only limited portions of the subsurface of each landslide, while the H/V technique was used to acquire a more complete data distribution over the entire landslide. The results of the active techniques were employed to constrain the seismic noise dataset (using Nakamura 1989 equation) and to obtain and validate H/V sections (here only shown for the Manaihan landslide). In all three landslides, the lithological contact of the upper Cretaceous sediments (sub-horizontal Vaals and Aachen layers) lying on top of the upper Carboniferous sediments was identified at a depth that ranges between ~10 and 30 m below surface. This interface is highly likely to represent the surface along which the sliding movement predominantly occurs. The integration of all the geophysical methods made it possible to reconstruct the 3D geological model of the Manaihan landslide.

Author contribution

Conceptualization, A.I., AS.M, L.C., HB.H., V.P.; methodology, A.I., AS.M, L.C., V.P.; investigation, A.I., AS.M, D.C, V.D., Y.H, HB.H.; data curation, A.I., AS.M, L.C., V.P.; writing original draft preparation, A.I., AS.M, L.C., V.P.; writing–review and editing, A.I., AS.M, L.C., D.C., V.D., Y.H, HB.H, V.P.; visualisation, A.I., AS.M, L.C., V.P.; supervision, V.P, HB.H; project administration, HB.H; funding acquisition, HB.H. All authors have read and agreed to the published version of the manuscript.

Funding

No research funds have been received.

Data availability

Data will be made available on request.

Declarations

Conflict of interest The authors declare no competing interests.

References

Alexandre P, Kusman D, Petermans T, Camelbeeck T (2008) The 18 September 1692 earthquake in the belgian ardenne and its aftershocks. In: Fréchet J, Meghraoui M, Stucchi M (eds) Historical seismology. Mod Approaches Solid Earth Sci (vol 2). Springer, Dordrecht. https://doi.org/10.1007/978-1-4020-8222-1_10

Ancion C, Evrard E (1957) Contribution à l'étude des failles Monty, Mouhy et d'Ostende dans la partie orientale du Massif de Herve. Ann Soc Geol Belg 80:477–488

Anomohanran O (2013) Seismic refraction method: a technique for determining the thickness of stratified substratum. Am J Appl Sci 10(8):857

Ayolabi EA, Adeoti L, Oshinlaja NA, Adeosun IO, Idowu OI (2009) Seismic refraction and resistivity studies of part of Igbogbo township, southwest Nigeria. J Scient Res Dev 11:42–61

Balasco M, Lapenna V, Rizzo E, Telesca L (2022) Deep electrical resistivity tomography for geophysical investigations: the state of the art and future directions. Geosci 12(12):438

Barchy L, Marion JM (2000) Carte géologique de Wallonie échelle 1/25.000, Dalhem-Herve 42/3-4

Bièvre G, Jongmans D, Chambert P, Schwartz S, Orengo Y, Beaurez N (2012) Geophysical study of a deep-seated landslide in a clay-shale terrain using ERT and MASW: Avignonet French Alps. Eng Geol 128:30–43. https://doi.org/10.1016/j.enggeo.2011.11.003

Calamita G, Gallipoli M, Gueguen E, Sinisi R, Summa V, Vignola L, Stabile T, Bellanova J, Piscitelli S, Perrone A (2023) Integrated geophysical and geological surveys reveal new details of the large Montescaglioso (southern Italy) landslide of December 2013. Eng Geol. https://doi.org/10.1016/j.enggeo.2023.106984

Castellaro S (2016) The complementarity of H/V and dispersion curves. Geophys 81(6):323–338

Chandler RJ (1986) ' Processes leading to landslides in clay slopes: a review', in A. D. Abrahams (Ed.), Hillslope Processes, Allen and Unwin, Winchester, Massachusetts, 344–360

Chen Y, Li L, Li J, Li G (2008) Wenchuan earthquake: way of thinking is changed. Episodes J Int Geosc 31(4):374–377

Dahlin T, Zhou B (2004) A numerical comparison of 2D resistivity imaging with 10 electrode arrays. Geophysical prospecting 52(5):379–398

Dal Moro G, Panza GF (2022) Multiple-peak HVSR curves: Management and statistical assessment. Engineering Geology 297:106500
Delgado J, Lopez Casado C, Giner J, Estevez A, Cuenca A, Molina S (2000) Microtremors as a geophysical exploration tool: applications and limitations. Pure Appl Geophys 157:1445–1462
Demanet D (2000) Tomographies 2D et 3D à partir de mesures géophysiques en surface et en forage, Ph. D. Thesis, Liege University, Belgium
Demoulin A (1988) Cenozoic tectonics on the Hautes Fagnes plateau (Belgium). Tectonophysics 145(1–2):31–41
Demoulin A, Chung C (2007) Mapping landslide susceptibility from small datasets: a case study in the Pays de Herve (E Belgium). Geomorphology 89(3–4):391–404
Demoulin A, Glade T (2004) Recent landslide activity in Manaihan East Belgium. Landslides 1(4):305–310
Demoulin A, Pissart A, Schroeder C (2003) On the origin of late quaternary palaeolandslides in the Liège (E-Belgium) area. Int J Earth Sci 92(5):795–805
Demoulin A, Delvenne Y, Juvigné E (2004) Les cours hypothétiques de la Warche pendant le Tertiaire et le Quartenaire ancien. Hautes Fagnes 3:80–83
Dindar H, Alevkayalı Ç (2023) Determination of GIS-based landslide susceptibility and ground dynamics with geophysical measurements and machine learning algorithms. Int J Geosynth Ground Eng 9(4):52
Forchap EA, Schmid G (1998) Experimental determination of Rayleigh-wave mode velocities using the method of wave number analysis. Soil Dyn Earthq Eng 17(3):177–183. https://doi.org/10.1016/S0267-7261(97)00039-0
Forir H (1905) Le pays de Herve. Essai de géographie physique. Ann Soc Geol Belg 33:163–171
Foti S (2005) Surface wave testing for geotechnical characterization. In: Lai CG, Wilmański K (eds) Surface waves in geomechanics: direct and inverse modelling for soils and rocks. CISM International Centre for Mechanical Sciences. Springer, Vienna, p 481. https://doi.org/10.1007/3-211-38065-5_2
Grandjean G, Monnet R, Bitri A (2009) Landslide characterization with geophysical data fusion: results from the Super-Sauze earthflow. J Appl Geophys 68(3):412–421. https://doi.org/10.1016/j.jappgeo.2008.04.002
Graulich JM (1969) La géologie de l'autoroute Liège-Aachen entre Herve et La Saute (Clermont). Ministère des affaires économiques, Administration des mines, Service géologique de Belgique
Hungr O, Leroueil S, Picarelli L (2014) The varnes classification of landslide types an update. Landslides 11(2):167–194
Ibs-von Seht M, Wohlenberg J (1999) Microtremor measurements used to map thickness of soft sediments. Bull Seismol Soc Am 89(1):250–259
Innocenti A, Rosi A, Tofani V, Pazzi V, Gargini E, Masi EB, Segoni S, Bertolo D, Paganone M, Casagli N (2023) Geophysical surveys for geotechnical model reconstruction and slope stability modelling. Remote Sens 15(8):2159
Innocenti A, Pazzi V, Borselli L, Nocentini M, Lombardi L, Gigli G, Fanti R (2023) Reconstruction of the evolution phases of a landslide by using multi-layer back-analysis methods. Landslides 20(1):189–207
Kabeta WF, Tamiru M, Tsige D, Ware H (2023) An integrated geotechnical and geophysical investigation of landslide in Chira Town Ethiopia. Heliyon. https://doi.org/10.1016/j.heliyon.2023.e17620
Konno K, Ohmachi T (1998) Ground-motion characteristics estimated from spectral ratio between horizontal and vertical components of microtremor. Bull Seismol Soc Am 88(1):228–241
Laloux M, Dejonghe L, Ghysel P, Hance L (1996) Notice explicative de la feuille Fléron-Verviers 42/7-8. Carte géologique de Wallonie à 1/25000, pp 1–150
Lapenna V, Perrone A (2022) Time-lapse electrical resistivity tomography (TL-ERT) for landslide monitoring: recent advances and future directions. Appl Sci 12(3):1425
Lin CP, Lin CH, Wu PL, Liu HC, Hung YC (2015) Applications and challenges of near surface geophysics in geotechnical engineering. Chin J Geophys 58(8):2664–2680
Loke MH (2004) Tutorial: 2-D and 3-D electrical imaging surveys
Lotti A, Pazzi V, Saccorotti G, Fiaschi A, Matassoni L, Gigli G (2018) HVSR analysis of rockslide seismic signals to assess the subsoil conditions and the site seismic response. Int J Geophys. https://doi.org/10.1155/2018/9383189
Luhn J, Stumvoll-Schmaltz MJ, Orozco AF, Glade T (2023) Internal structure of an active landslide based on ERT and DP data: new insights from the Hofermühle landslide observatory in lower Austria. Geomorphology. https://doi.org/10.1016/j.geomorph.2023.108910
Merritt A, Chambers J, Murphy W, Wilkinson P, West L, Gunn D, Meldrum P, Kirkham M, Dixon N (2014) 3D ground model development for an active landslide in Lias mudrocks using geophysical remote sensing and geotechnical methods. Landslides 11:537–550
Molnar S, Sirohey A, Assaf J, Bard PY, Castellaro S, Cornou C, Cox B, Guillier B, Hassani B, Kawase H et al (2022) A review of the microtremor horizontal-to-vertical spectral ratio (MHVSR) method. J Seismol 26(4):653–685
Montrasio L, Valentino R (2007) Experimental analysis and modelling of shallow landslides. Landslides 4:291–296. https://doi.org/10.1007/s10346-007-0082-3
Mreyen AS, Demoulin A, Havenith HB (2018) Seismotectonic activity in east Belgium: relevance of a major scarp and two associated landslides in the region of Malmedy. Geol Belg 21(3–4):101–110
Mreyen AS, Cauchie L, Micu M, Onaca A, Havenith HB (2021) Multiple geophysical investigations to characterize massive slope failure deposits: application to the Balta rockslide Carpathians. Geophys J Int 225(2):1032–1047
Nakamura Y (1989) A method for dynamic characteristics estimation of subsurface using microtremor on the ground surface. Railway Technical Research Institute, Quarterly Reports, 30(1)
Okada H, Suto K (2003) The microtremor survey method. Society of Exploration Geophysicists. https://doi.org/10.1190/1.9781560801740
Panzera F, D'Amico S, Lotteri A, Galea P, Lombardo G (2012) Seismic site response of unstable steep slope using noise measurements: the case study of Xemxija bay area Malta. Nat Hazard 12(11):3421–3431. https://doi.org/10.5194/nhess-12-3421-2012
Park CB, Miller RD, Xia J (1999) Multichannel analysis of surface waves. Geophysics 64(3):800–808
Patrizi G, Guidi G, Ciani L, Catelani M, Cappuccini L, Innocenti A, Casagli N, Pazzi V (2022) Analysis of non-ideal remote pole in electrical resistivity tomography for subsurface surveys. In: 2022 IEEE international instrumentation and measurement technology conference (I2MTC), IEEE , pp 1–5
Pazzi V, Tanteri L, Bicocchi G, D'Ambrosio M, Caselli A, Fanti R (2017) H/V measurements as an effective tool for the reliable detection of landslide slip surfaces: case studies of Castagnola (La Spezia, Italy) and Roccalbegna (Grosseto Italy). Phys Chem Earth Parts A/B/C 98:136–153
Pazzi V, Ceccatelli M, Gracchi T, Masi EB, Fanti R (2018) Assessing subsoil void hazards along a road system using H/V measurements ERTS and IPTS to support local decision makers. Near Surf Geophys 16(3):282–297
Pazzi V, Filippo M, Nezza M, Carlà T, Bardi F, Marini F, Fontanelli K, Intrieri E, Fanti R (2018) Integrated geophysical survey in a sinkhole-prone area: microgravity electrical resistivity tomographies and seismic noise measurements to delimit its extension. Eng Geol 243:282–293
Pazzi V, Ceccatelli M, Ciani L, Patrizi G, Guidi G, Cappuccini L, Casagli N, Catelani M (2020) Analysis of the influence of the GPS errors occurred while collecting electrode coordinates on the electrical resistivity of Tumuli. Sensors 20(10):2966
Pazzi V, Morelli S, Fanti R (2019) A review of the advantages and limitations of geophysical investigations in landslide studies. Int J Geophys. https://doi.org/10.1155/2019/2983087
Perrone A, Canora F, Calamita G, Bellanova J, Serlenga V, Panebianco S, Tragni N, Piscitelli S, Vignola L, Doglioni A et al (2021) A multidisciplinary approach for landslide residual risk assessment: the Pomarico landslide (Basilicata region Southern Italy) case study. Landslides 18:353–365
Persichillo MG, Bordoni M, Meisina C, Bartelletti C, Barsanti M, Giannecchini R, D'Amato Avanzi G, Galanti Y, Cevasco A, Brandolini P et al (2017) Shallow landslides susceptibility assessment in different environments. Geomatics Nat Hazards Risk 8(2):748–771. https://doi.org/10.1080/19475705.2016.1265011

Preuth T, Glade T, Demoulin A (2010) Stability analysis of a human-influenced landslide in eastern Belgium. Geomorphology 120(1):38–47. https://doi.org/10.1016/j.geomorph.2009.09.013
Redpath BB (1973) Seismic refraction exploration for engineering site investigations (No. EERL-TR-E--73-4). Army Engineer Waterways Experiment Station, Livermore, Calif.(USA). Explosive Excavation Research Lab
Santarato G, Ranieri G, Occhi M, Morelli G, Fischanger F, Gualerzi D (2011) Three-dimensional electrical resistivity tomography to control the injection of expanding resins for the treatment and stabilization of foundation soils. Eng Geol 119(1–2):18–30
Seitone F, Vergnano A, Comina C, Bonasera M, Fubelli G (2025) Comparative analysis of geological and seismic microtremors models of a large translational landslide: the case of San Vito Romano (Central Italy). Eng Geol 107934. https://doi.org/10.1016/j.enggeo.2025.107934
Sendrós A, Himi M, Lovera R, Rivero L, Garcia-Artigas R, Urruela A, Casas A (2020) Geophysical characterization of hydraulic properties around a managed aquifer recharge system over the Llobregat River Alluvial Aquifer (Barcelona metropolitan area). Water 12(12):3455
Site EffectS Assessment using AMbient Excitations (SESAME) (2004) Guidelines for the implementation of the H/V spectral ratio technique on ambient vibrations measurements, processing and interpretation, SESAME European Research Project , WP12 - Deliverable D23.12
Sgattoni G, Castellaro S (2020) Detecting 1-d and 2-d ground resonances with a single-station approach. Geophys J Int 223(1):471–487
Song C, Yu C, Li Z, Pazzi V, Soldato M, Cruz A, Utili S (2021) Landslide geometry and activity in Villa de la Independencia (Bolivia) revealed by InSAR and seismic noise measurements. Landslides 18(8):2721–2737. https://doi.org/10.1007/s10346-021-01659-9
Uhlemann S, Smith A, Chambers J, Dixon N, Dijkstra T, Merritt A, Swift R, Mainsant G, Whiteley J (2017) Evaluation of ground-based geophysical techniques for long-term monitoring of landslides. Geomorph 283:150–167. https://doi.org/10.1016/j.geomorph.2017.01.029
Vivaldi V, Torrese P, Bordoni M, Viglietti F, Meisina C (2024) ERT-based experimental integrated approach for soil hydrological characterization in rainfall-induced shallow landslides prone areas. Bull Eng Geol Env 83(5):167
Vivoda Prodan M, Peranić J, Pajalić S (2023) Arbanas Ž (2023) Physical modelling of rainfall-induced sandy and clay-like slope failures. Adv Mater Sci Eng 1:3234542. https://doi.org/10.1155/2023/3234542
Wathelet M, Jongmans D, Ohrnberger M, Bonnefoy-Claudet S (2008) Array performances for ambient vibrations on a shallow structure and consequences over Vs inversion. J Seismol 12(1):1–19
Wei Y, Shi Z, Wang C, Huang M (2024) Joint imaging of ERT datasets and its application in seepage characterization at Nanshan Dam southeast China. J Appl Geophys. https://doi.org/10.1016/j.jappgeo.2024.105390
Whiteley J, Chambers J, Uhlemann S, Wilkinson PB, Kendall J (2019) Geophysical monitoring of moisture-induced landslides: a review. Rev Geophys 57(1):106–145
Yalcin A (2007) The effects of clay on landslides: a case study. Appl Clay Sci 38(1–2):77–85
Zhang G, Tu F, Tang Y, Chen X, Xie K, Dai S (2023) Application of geophysical prospecting methods ERT and MASW in the landslide of Daofu County China. Front Earth Sci 10:1054394

Agnese Innocenti (✉) · Veronica Pazzi
Department of Earth Sciences, University of Florence, Firenze 50121, Italy
Email: agnese.innocenti@unifi.it

Anne-Sophie Mreyen · David Caterina
Urban and Environmental Engineering, University of Liege, Liege 4000, Belgium

Léna Cauchie
ULiege Library, Faculty of Sciences, University of Liege, Liege 4000, Belgium

Valmy Dorival · Hans-Balder Havenith
Department of Geology, University of Liege, Liege 4000, Belgium

Yawar Hussain
Department of Sustainable Earth Systems Sciences, The University of Texas at Dallas, Richardson, TX 75080-3021, USA